

Single orthorhombic b axis orientation and antiferromagnetic ordering type in multiferroic CaMnO_3 thin film with $\text{La}_{0.67}\text{Ca}_{0.33}\text{MnO}_3$ buffer layer

F. Wang, B. J. Dong, Y. Q. Zhang, W. Liu, H. R. Zhang, Y. Bai, S. K. Li, T. Yang, J. R. Sun, Z. J. Wang, and Z. D. Zhang

Citation: *Appl. Phys. Lett.* **111**, 122902 (2017);

View online: <https://doi.org/10.1063/1.5003815>

View Table of Contents: <http://aip.scitation.org/toc/apl/111/12>

Published by the [American Institute of Physics](#)

Articles you may be interested in

[Voltage control of spin wave resonance in \$\text{La}_{0.5}\text{Sr}_{0.5}\text{MnO}_3/\text{PMN-PT}\$ \(001\) multiferroic heterostructures](#)

Applied Physics Letters **111**, 102903 (2017); 10.1063/1.4990545

[Electric field modulated conduction mechanism in \$\text{Al}/\text{BaTiO}_3/\text{La}_{0.67}\text{Sr}_{0.33}\text{MnO}_3\$ heterostructures](#)

Applied Physics Letters **111**, 062901 (2017); 10.1063/1.4997412

[Room temperature multiferrocity and magnetodielectric properties of ternary \(1-x\) \$\(0.94\text{Bi}_{0.5}\text{Na}_{0.5}\text{TiO}_3-0.06\text{BaTiO}_3\)\$ - \$x\text{BiFeO}_3\$ \(\$0 \leq x \leq 0.9\$ \) solid solutions](#)

Applied Physics Letters **111**, 112902 (2017); 10.1063/1.4986360

[Periodic arrays of flux-closure domains in ferroelectric thin films with oxide electrodes](#)

Applied Physics Letters **111**, 052901 (2017); 10.1063/1.4996232

[On the inter-layer magneto-electric coupling in \$\text{BiFeO}_3/\text{SrRuO}_3\$ heterostructure](#)

Applied Physics Letters **111**, 102902 (2017); 10.1063/1.5001480

[Oxygen deficiency and cooling field driven vertical hysteretic shift in epitaxial \$\text{SrRuO}_3/\text{SrTiO}_3\$ heterostructures](#)

Applied Physics Letters **111**, 152405 (2017); 10.1063/1.5000866

Scilight

Sharp, quick summaries **illuminating**
the latest physics research

Sign up for **FREE!**

AIP
Publishing

Single orthorhombic b axis orientation and antiferromagnetic ordering type in multiferroic CaMnO_3 thin film with $\text{La}_{0.67}\text{Ca}_{0.33}\text{MnO}_3$ buffer layer

F. Wang,^{1,2} B. J. Dong,^{1,2} Y. Q. Zhang,¹ W. Liu,^{1,a)} H. R. Zhang,^{2,3} Y. Bai,¹ S. K. Li,¹ T. Yang,¹ J. R. Sun,³ Z. J. Wang,¹ and Z. D. Zhang¹

¹Shenyang National Laboratory for Materials Science, Institute of Metal Research, Chinese Academy of Sciences, 72 Wenhua Road, Shenyang 110016, China

²University of Chinese Academy of Sciences, Beijing 100049, China

³Beijing National Laboratory for Condensed Matter, Institute of Physics, Chinese Academy of Sciences, Beijing 100190, China

(Received 27 May 2017; accepted 7 September 2017; published online 19 September 2017)

The detailed crystal structure and antiferromagnetic properties of a 42 nm thick CaMnO_3 film grown on a LaAlO_3 substrate with a 9 nm $\text{La}_{0.67}\text{Ca}_{0.33}\text{MnO}_3$ buffer layer have been investigated. Compared with a CaMnO_3 film directly grown on a LaAlO_3 substrate, only one kind of orthorhombic b axis orientation along the [100] axis of the substrate is observed in the CaMnO_3 film with a $\text{La}_{0.67}\text{Ca}_{0.33}\text{MnO}_3$ buffer layer. To determine the antiferromagnetic ordering type of our CaMnO_3 film with a buffer layer, the first-principles calculations were carried out with the results, indicating that the CaMnO_3 film, even under a tensile strain of 1.9%, is still a compensated G-type antiferromagnetic order, the same as the bulk. Moreover, the exchange bias effect is observed at the interface of the $\text{CaMnO}_3/\text{La}_{0.67}\text{Ca}_{0.33}\text{MnO}_3$ film, further confirming the antiferromagnetic ordering of the CaMnO_3 film with a buffer layer. In addition, it is concluded that the exchange bias effect originates from the spin glass state at the $\text{La}_{0.67}\text{Ca}_{0.33}\text{MnO}_3/\text{CaMnO}_3$ interface, which arises from a competition between the double-exchange ferromagnetic $\text{La}_{0.67}\text{Ca}_{0.33}\text{MnO}_3$ and super-exchange antiferromagnetic CaMnO_3 below the spin glass freezing temperature. *Published by AIP Publishing.*

[<http://dx.doi.org/10.1063/1.5003815>]

Single phase perovskite multiferroic materials with an ABO_3 structure have been attracting attention from both the fundamental physics study and technological applications in recent years.^{1–3} However, within the empirical “ d^0 -ness” rule, the magneto-electric couple is always limited by ferroelectricity and magnetism originating from different lattice sites. For example, in EuTiO_3 ,^{4,5} ferroelectricity originates from the off-centering of B (Ti^{4+}) sites, while magnetism stems from the 4f moment of A (Eu^{2+}) magnetic cation sites. In BiMnO_3 , magnetism arises from B (Mn^{3+}) magnetic ion sites, while ferroelectricity results from the 6s electron lone pair of A (Bi^{3+}) sites.⁶ To enhance the coupling between electric polarization and magnetization, it is suggested that they can be driven by the same cation site.^{7,8} Recent first principles calculation shows that both antiferromagnetism and ferroelectricity can be associated with the Mn^{4+} cation in the tensile-strained perovskite RMnO_3 (R = Ca, Sr, and Ba) films.^{9–11}

Bulk CaMnO_3 (CMO) possesses G-type antiferromagnetic (AFM) ordering with a Néel temperature of 125 K and is non-polar. It has been reported in Ref. 9 that strain can induce ferroelectricity in CMO. Actually, the emergence of polarity in CMO epitaxial films grown directly on a LaAlO_3 substrate has been observed below 25 K by second harmonic generation measurements.¹² However, it is noticed that in the above CMO films, there are three different domains associated with three different orientations of the orthorhombic unit cell of CMO with respect to the substrate, namely, the

orthorhombic b axis is along the x, y, or z direction of the substrate.

It has been reported that the use of a buffer layer is an effective method to control the rotations of oxygen octahedral in perovskite oxide films. For example, the insertion of a SrTiO_3 buffer at the $\text{La}_{2/3}\text{Sr}_{1/3}\text{MnO}_3/\text{NdGaO}_3$ interface changes the octahedral tilt and rotation in the $\text{La}_{2/3}\text{Sr}_{1/3}\text{MnO}_3$ layer, leading to a reorientation of the magnetic easy axis.¹³ The introduction of a BaTiO_3 buffer layer at the $\text{SrRuO}_3/\text{GdScO}_3$ interface results in a stable tetragonal structure in the SrRuO_3 film rather than the monoclinic structure when grown directly on a GdScO_3 substrate.¹⁴ Considering that bulk $\text{La}_{0.67}\text{Ca}_{0.33}\text{MnO}_3$ (LCMO) has the same crystal structure as bulk CMO and is a better match with CMO with respect to the Mn-O-Mn bond angle, a 9-nm-thick buffer layer LCMO was inserted between the CMO/ LaAlO_3 interface to induce a single orthorhombic b axis orientation in the whole CMO film. In addition, the LCMO buffer layer is ferromagnetic (FM), which also brings the possibility to prove that the CMO film is antiferromagnetic (AFM) through the exchange bias effect at the interface of the CMO/LCMO bilayer.

It is well known that the epitaxial strain affects not only the Néel temperature but also the AFM ordering type of the perovskite oxide films by tuning the c/a ratio of the unit cell.^{15–17} In our paper, we investigate the growth and crystal structure of the CMO film with buffer layer LCMO. We carry out the first-principles calculation to determine the AFM ordering type of CMO film under a tensile strain of 1.9% and then investigate the exchange bias effect and its origin at the interface of LCMO/CMO bilayers in detail.

^{a)}Author to whom correspondence should be addressed: wliu@imr.ac.cn

42 nm CMO films with a buffer layer of 9 nm LCMO (referred hereafter to as the b-CMO film) were grown on (001)-oriented LaAlO_3 substrates by pulsed laser deposition. As reference samples, the LCMO and CMO single layers were grown under the same conditions. The energy fluency of the laser is approximately 1.5 J/cm^2 , and the frequency is 2 Hz. All films were deposited on a LaAlO_3 substrate at an oxygen pressure of 0.4 mbar and at a substrate temperature of 750°C . Then, they were annealed in an oxygen atmosphere of 0.5 bar for 2 h to remove oxygen vacancies. Coherent epitaxial growth, detail crystal structure, and film orientation were analyzed using a high resolution transmission electric microscope (HRTEM) and X-ray diffraction (XRD). The measurements of magnetic properties were performed using a superconducting quantum interference device magnetometer (SQUID). In all magnetic measurements in our paper, the magnetic field was applied along the in-plane direction of the thin film.

The bulk CMO crystal is a distorted orthorhombic structure with space group $Pnma$, with the lattice parameters of $a = 5.279 \text{ \AA}$, $b = 7.448 \text{ \AA}$, and $c = 5.264 \text{ \AA}$.¹² For the calculation of lattice mismatch between bulk CMO and substrate, it is often described as a pseudo-cubic perovskite structure with a lattice parameter of $a/\sqrt{2} \approx b/2 \approx c/\sqrt{2} \approx a_{\text{cubic}} = 3.72 \text{ \AA}$. The (001)-oriented single crystal LaAlO_3 substrate with a pseudo-cubic in-plane lattice constant of 3.79 \AA was used to induce a nominal epitaxial strain of 1.9% in the CMO film. Figure 1(a) shows the out-of-plane XRD pattern of the b-CMO film grown on a (001)-oriented LaAlO_3 substrate. Only (001) reflections of both the CMO layer and LCMO layer are observed, suggesting a c-axis orientation of the b-CMO film. Figure 1(b) shows symmetric X-ray reciprocal space maps (RSM) of the b-CMO film and substrate around the $(\bar{1}03)$ diffraction peaks (no spots in RSM for the LCMO layer are detected due to its small thickness of 9 nm). It is found that the CMO layer is fully strained with lattice constants of $a = b = 3.79 \text{ \AA}$ and $c = 3.71 \text{ \AA}$.

Figure 1(d) shows the HRTEM image of the b-CMO film. Clear and well-defined interfaces (marked by a dotted line) are observed not only between the CMO layer and the LCMO layer but also between the LCMO layer and the LaAlO_3 substrate. Figures 1(e) and 1(f) show the Fourier transformation patterns of the CMO layer and LCMO layer, respectively. It can be seen that, compared with the simple orthorhombic structure of the LCMO layer, additional reflections of the CMO layer (marked by red color) are observed due to MnO_6 octahedral distortion and rotation about the orthorhombic b axis. Moreover, the orthorhombic b axis is only along the [100] direction of the LaAlO_3 substrate. For comparison, the TEM measurement was also carried out for the CMO film grown directly on a LaAlO_3 substrate, and the HRTEM image is shown in Fig. 1(c). Similar to results previously reported,¹² the Fourier transformation pattern (not shown here) reveals three different regions (marked by colored circles) in the HRTEM image of the CMO film corresponding to three different orthorhombic b axis orientations along the x, y, or z direction of the LaAlO_3 substrate. This clearly indicates that the LCMO buffer layer induces the single orthorhombic b axis orientation in the top CMO layer. The main reason for this phenomena may be ascribed to the following: (1) The LaAlO_3 substrate has a rhombohedral crystal structure with the $R\bar{3}c$ space group, whereas the LCMO and CMO have the same $Pnma$ orthorhombic structure; and (2) the magnitude of the CMO bond angle (156°) has a lower mismatch with LCMO (163°) than that of the LaAlO_3 (171.4°) substrate. The crystallographic symmetry-match and the smaller difference in the bond angle of LCMO and CMO will lead to a strengthened oxygen octahedral coupling and the formation of a single orthorhombic b axis orientation in the CMO layer. In addition to the crystallographic symmetry-match and octahedral bonding angle, the strain is also crucial to determine the oxygen octahedral rotations. Although a LCMO buffer layer was inserted at the CMO/ SrTiO_3 interface, the multi-domain state with three different

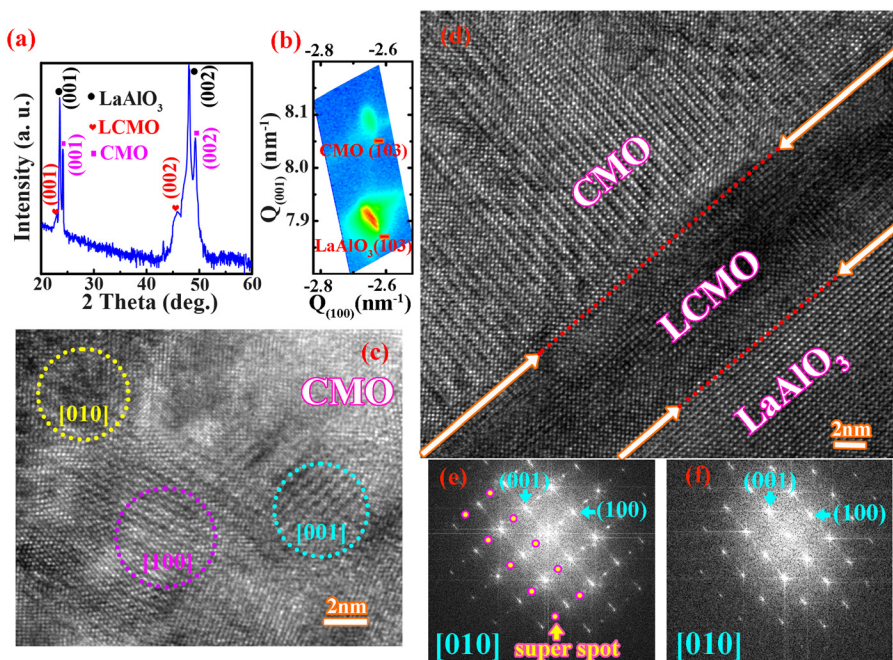


FIG. 1. (a) θ - 2θ XRD scans of the b-CMO film on a (001) LaAlO_3 substrate. (b) Reciprocal space maps around the $(\bar{1}03)$ reflections of the b-CMO film and LaAlO_3 substrate. (c) Cross-sectional HRTEM image of the CMO film directly grown on a LaAlO_3 substrate along the direction [010] zone axis of substrate LaAlO_3 . (d) Cross-sectional HRTEM image of the b-CMO film along the direction [010] zone axis of substrate LaAlO_3 . (e) Fast Fourier transform patterns of the CMO layer in the b-CMO film. (f) Fast Fourier transform patterns of the LCMO layer in the b-CMO film.

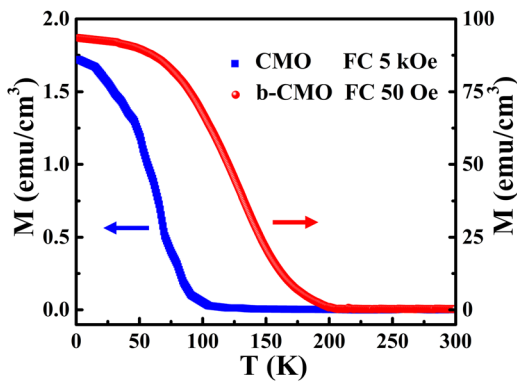


FIG. 2. The temperature dependence of the magnetization of the b-CMO film under a magnetic field of 50 Oe and reference CMO single layer under a magnetic field of 5 kOe.

b axis orientations would be formed inevitably.¹⁸ It is concluded that the formation of the single orthorhombic b axis is closely related to epitaxial strain, crystallographic symmetry-(mis)match, and the octahedral bonding angle and length at the interfaces.

As introduced above, bulk CMO has a G-type AFM ordering with Néel temperature, T_N , near 125 K. Figure 2 shows the temperature dependent magnetization of both the b-CMO and the CMO film directly grown on a LaAlO_3 substrate. It is seen from Fig. 2 that T_N is around 100 K in the CMO film directly grown on the LaAlO_3 substrate, which is similar to a previous report,¹⁵ indicating that the AFM ordering temperature is suppressed in the tensile strained CMO film compared to the bulk. For the b-CMO film, the T_N of the CMO layer cannot be detected due to a strong ferromagnetic signal of the LCMO layer, and the Curie temperature of the LCMO layer is observed to be around 200 K. As mentioned above, epitaxial strain may change the AFM ordering type in a perovskite oxide film, so we wonder if the AFM ordering type of the CMO layer in our b-CMO film, under a tensile strain of 1.9%, is still the same as the bulk and is G-type AFM ordering. It is noted the AFM ordering type of the CMO film under epitaxial strain was not clearly defined thus far although its AFM behavior was demonstrated by an adjacent FM layer.^{18,19}

To explore the effect of lattice strain on the AFM ordering type of the CMO layer in the b-CMO film, first-principles

density functional calculations were performed within the generalized gradient approximation GGA + U method^{20,21} as implemented in the Vienna *ab initio* simulation package.²² The on-site Coulomb interaction $U = 2.7$ eV and exchange interaction $J_H = 1$ eV were used to treat the localized d electron for the Mn ion, from which a good agreement with the experimental magnetic moment of Mn ion is obtained.^{10,23} The projector-augmented-wave pseudopotentials²⁴ and the Perdew-Burke-Ernzerhof²⁵ exchange-correlation functional were used. The experimental lattice constants of the CMO layer ($a = b = 3.79$ Å) were adopted in our calculations. In order to simulate different antiferromagnetic ground states of CMO at the (001) surface, a $2 \times 2 \times 1$ supercell was used, where an 18 Å vacuum space was added in the $\langle 001 \rangle$ direction to avoid the inter-surface interaction. The lattice constants were $a = b = 7.58$ Å and $c = 25$ Å as shown in Fig. 3(a). The Brillouin zone of the super cell was sampled by a $4 \times 4 \times 1$ k-point mesh. The electronic kinetic-energy cutoff for the plane-wave basis was set to be 500 eV, and a total-energy difference below 10^{-4} eV between subsequent electronic iterations was set as the criterion of self-consistency. All geometries have been optimized using the conjugate-gradient method,²⁶ until none of the residual Hellmann-Feynman forces exceed 10^{-2} eV/Å. In order to get the ground-state spin structure, we start from four common spin states (FM, A-type AFM, G-type AFM, and C-type AFM), as shown in Fig. 3(b). The most stable spin structure from our energy calculations is the G-type AFM, as highlighted by the dashed frame in Fig. 3(b). The order of the relative stability of these spin states are G-type AFM > C-type AFM > A-type AFM > FM with the energy difference around 9–60 meV per CMO formula unit between the G-type and others. The spin moment at each Mn site at the interface is $2.681 \mu_B$. The Mn sublayer below the interface Mn layer is also in a G-type AFM order but with a slightly smaller spin moment ($2.525 \mu_B$). Our first-principles calculation results indicate that the top CMO layer maintains a compensated G-type AFM spin order under a tensile strain of 1.9%.

Figure 4(a) shows the hysteresis loops of the b-CMO film and the reference LCMO single layer measured at 4 K after field cooling from room temperature. It is seen from Fig. 4(a) that the hysteresis loops shift along the magnetic-field

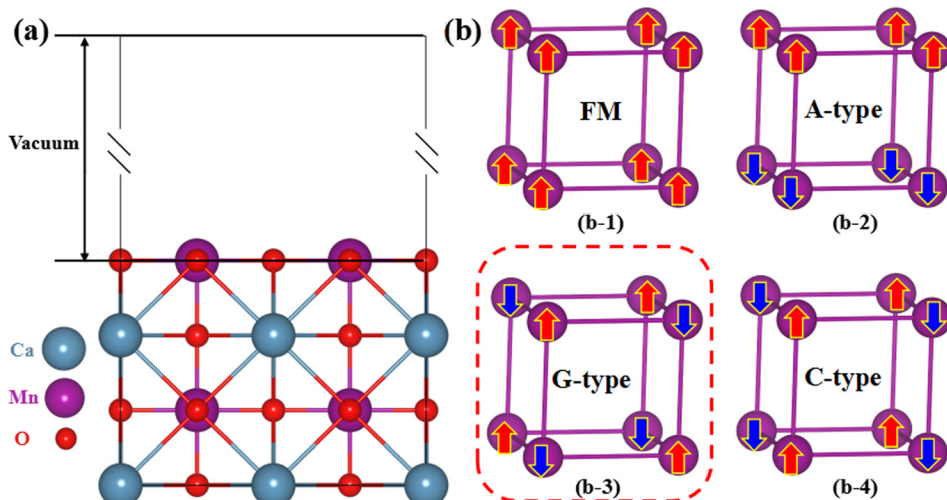


FIG. 3. Relative stability of spin states on the CMO surface. (a) Atomic surface structure of CMO. (b) Four typical spin states: (b-1) FM, (b-2) A-type AFM, (b-3) G-type AFM, and (b-4) C-type AFM. The G-type highlighted in the red dashed frame is relatively more stable than the other three types.

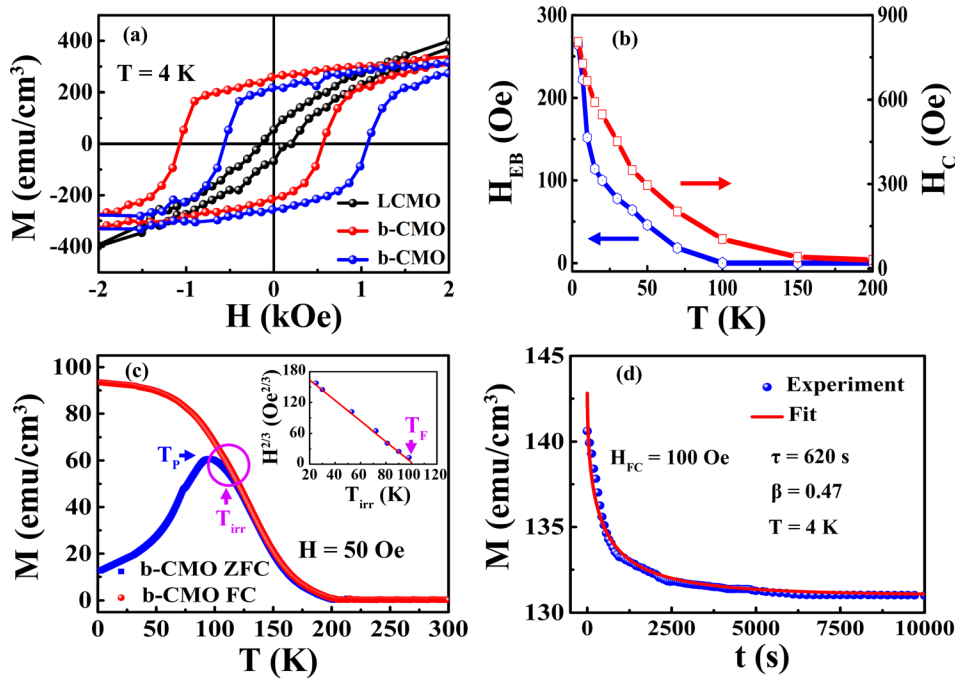


FIG. 4. (a) Magnetic hysteresis loops of the b-CMO film at 4 K after the cooling field in the magnetic fields of +4 kOe and -4 kOe and the LCMO single layer after the cooling filed in a magnetic field of +4 kOe. The measurement range is between -20 kOe and 20 kOe. For clarity, only the data between -2 kOe and +2 kOe is shown. (b) The temperature dependence of the exchange bias field and coercive field of the b-CMO film. (c) ZFC and FC curves of the b-CMO film at 50 Oe. The inset shows the field dependence of irreversibility temperature T_{irr} and fitted Almeida-Thouless line. (d) The time dependence of the thermal remnant magnetization after the cooling field under a magnetic field of 100 Oe from room temperature to 4 K.

axis, indicating that the exchange bias effect exists in this b-CMO film. The absolute values of the exchange bias field (H_{EB}) and coercivity (H_C) are calculated using $H_{EB} = |H_1 + H_2|/2$ and $H_C = |H_1 - H_2|/2$, where H_1 and H_2 are the values of the magnetic field at which the magnetization goes to zero. The shift of the hysteresis loops is found to be highly reversible with respect to the cooling field direction, namely, $H_{EB} \approx -260$ Oe and $H_{EB} \approx 270$ Oe correspond to the cooling field of +4 kOe and -4 kOe, respectively. However, no exchange bias effect is observed in the LCMO single layer at 4 K after +4 kOe field cooling from room temperature. So, the exchange bias phenomenon in the b-CMO film unambiguously stems from the interface coupling. The temperature dependence of H_{EB} and H_C are shown in Fig. 4(b). The exponential dependence of the thermal variation of H_{EB} and H_C are observed, which also has been reported in $La_{0.7}Sr_{0.3}MnO_3/SrMnO_3$, $La_{0.67}Sr_{0.33}MnO_3/BiFeO_3$, and $La_{0.7}Sr_{0.3}MnO_3/La_2CuO_4$ systems.²⁷⁻²⁹ This is a typical characteristic of the interface spin glass state, which generally originates from the competition between $Mn^{3+}-Mn^{4+}$ FM double-exchange and $Mn^{4+}-Mn^{4+}$ AFM super-exchange interactions in manganite oxide systems.²⁷⁻²⁹ Moreover, it is clearly seen in zero field cooling and field cooling (ZFC-FC) curves of the b-CMO film [as shown in Fig. 4(c)] that a peak temperature (T_p) in the ZFC curve and the irreversibility temperature (T_{irr}), below which a notable bifurcation between the ZFC curve and the FC curve occurs, are very close. This also suggests a spin glass behavior occurring at the LCMO/CMO interface. Similar ZFC-FC curves have also been observed at other applied fields. It is clear from the inset of Fig. 4(c) that the applied magnetic field dependence of the irreversibility temperature (T_{irr}) follows the Almeida-Thouless line²⁷ through fitting (marked by red line) by the following formula: $H(T_{irr})/\Delta J \propto (1 - T_{irr}/T_F)^{3/2}$, where T_F is the zero field freezing temperature and ΔJ is the width of the distribution of the exchange interaction. This is commonly observed in spin frustrated systems.^{19,27} To further confirm that the spin frustration in our paper is spin glass, we measured the frequency

dependence of ac susceptibility; however, the signal is too weak and it is difficult to get reliable data. We investigated the time dependence of the magnetic relaxation behavior at 4 K after 100 Oe field cooling as shown in Fig. 4(d). The decay curve can be fitted by a stretched-exponential function: $M = M_2 + (M_1 - M_2) \exp[-(t/\tau)^\beta]$, where M_2 and M_1 are the final and initial magnetizations, τ is the relaxation time, and β is the shape parameter. The fitting parameter β is determined to be 0.47, which is similar to the values reported for other spin glass systems.^{30,31} So, we believe that the spin frustration in our b-CMO film is a spin glass state.

In summary, we carried out detailed crystal structure and magnetic property studies of multiferroic CMO thin films with an LCMO buffer layer. Compared with CMO films directly grown on a $LaAlO_3$ substrate, it is found that the buffer LCMO layer favors a single orthorhombic b axis orientation throughout the CMO layer. First-principles calculations results indicate that the 1.9% tensile strained CMO layer is still G-type AFM ordering, the same as the bulk. The exchange bias effect observed at the interface between the CMO layer and the LCMO layer further confirms that the top CMO thin film is antiferromagnetic. However, whether it is G-type or not cannot be determined experimentally needs further neutron diffraction investigation in the future. Moreover, it is concluded that the above exchange bias effect originates from the spin glass state at the LCMO/CMO interface due to the competition between the $Mn^{3+}-Mn^{4+}$ FM double exchange interaction of the LCMO layer and the $Mn^{4+}-Mn^{4+}$ AFM super-exchange interaction of the CMO layer.

This work was supported by the National Nature Science Foundation of China under Project Nos. 51590883, 51271177, and 11520101002 and the project of Chinese Academy of Sciences under Grant No. KJZD-EW-M05-3.

¹Y. Tokura and S. Seki, *Adv. Mater.* **22**, 1554-1565 (2010).

²F. Wang, Y. Q. Zhang, W. Liu, X. K. Ning, Y. Bai, Z. M. Dai, S. Ma, X. G. Zhao, S. K. Li, and Z. D. Zhang, *Appl. Phys. Lett.* **106**, 232906 (2015).

- ³X. Li, C. L. Lu, J. Y. Dai, S. Dong, Y. Chen, N. Hu, G. H. Wu, M. F. Liu, Z. B. Yan, and J. M. Liu, *Sci. Rep.* **4**, 7019 (2014).
- ⁴X. Ke, T. Biroli, R. Misra, J.-H. Lee, B. J. Kirby, D. G. Schlom, C. J. Fennie, and J. W. Freeland, *Phys. Rev. B* **88**, 094434 (2013).
- ⁵C. J. Fennie and K. M. Rabe, *Phys. Rev. Lett.* **97**, 267602 (2006).
- ⁶T. Kimura, S. Kawamoto, I. Yamada, M. Azuma, M. Takano, and Y. Tokura, *Phys. Rev. B* **67**, 180401(R) (2003).
- ⁷H. Sakai, J. Fujioka, T. Fukuda, M. S. Bahramy, D. Okuyama, R. Arita, T. Arima, A. Q. R. Baron, Y. Taguchi, and Y. Tokura, *Phys. Rev. B* **86**, 104407 (2012).
- ⁸H. Sakai, J. Fujioka, T. Fukuda, D. Okuyama, D. Hashizume, F. Kagawa, H. Nakao, Y. Murakami, T. Arima, A. Q. R. Baron, Y. Taguchi, and Y. Tokura, *Phys. Rev. Lett.* **107**, 137601 (2011).
- ⁹S. Bhattacharjee, E. Bousquet, and P. Ghosez, *Phys. Rev. Lett.* **102**, 117602 (2009).
- ¹⁰J. H. Lee and K. M. Rabe, *Phys. Rev. Lett.* **104**, 207204 (2010).
- ¹¹C. Becher, L. Maurel, U. Aschauer, M. Lilienblum, C. Mageñ, D. Meier, E. Langenberg, M. Trassin, J. Blasco, I. P. Krug, P. A. Algarabel, N. A. Spaldin, J. A. Pardo, and M. Fiebig, *Nat. Nanotechnol.* **10**, 661 (2015).
- ¹²T. Günter, E. Bousquet, A. David, P. Boullay, P. Ghosez, W. Prellier, and M. Fiebig, *Phys. Rev. B* **85**, 214120 (2012).
- ¹³Z. Liao, M. Huijben, Z. Zhong, N. Gauquelin, S. Macke, R. J. Green, S. Van Aert, J. Verbeeck, G. Van Tendeloo, K. Held, G. A. Sawatzky, G. Koster, and G. Rijnders, *Nat. Mater.* **15**, 425 (2016).
- ¹⁴D. Kan, Y. Wakabayashi, H. Tajiri, and Y. Shimakawa, *Phys. Rev. B* **94**, 024112 (2016).
- ¹⁵C. L. Flint, A. J. Grutter, C. A. Jenkins, E. Arenholz, and Y. Suzuki, *J. Appl. Phys.* **115**, 17D712 (2014).
- ¹⁶L. Maurel, N. Marcano, T. Prokscha, E. Langenberg, J. Blasco, R. Guzman, A. Suter, C. Magen, L. Morellon, M. R. Ibarra, J. A. Pardo, and P. A. Algarabel, *Phys. Rev. B* **92**, 024419 (2015).
- ¹⁷F. Wang, Y. Q. Zhang, Y. Bai, W. Liu, H. R. Zhang, W. Y. Wang, S. K. Li, S. Ma, X. G. Zhao, J. R. Sun, Z. H. Wang, Z. J. Wang, and Z. D. Zhang, *Appl. Phys. Lett.* **109**, 052403 (2016).
- ¹⁸Z. H. Wang, G. Cristiani, H. U. Habermeier, and J. A. C. Bland, *Phys. Rev. B* **72**, 054407 (2005).
- ¹⁹F. Wang, Y. Bai, W. Liu, H. R. Zhang, S. K. Li, Z. M. Dai, S. Ma, X. G. Zhao, S. C. Wang, Z. J. Wang, and Z. D. Zhang, *J. Magn. Magn. Mater.* **428**, 372–376 (2017).
- ²⁰C. Loschen, J. Carrasco, K. M. Neyman, and F. Illas, *Phys. Rev. B* **75**, 035115 (2007).
- ²¹S. L. Dudarev, G. A. Botton, S. Y. Savrasov, C. J. Humphreys, and A. P. Sutton, *Phys. Rev. B* **57**, 1505 (1998).
- ²²G. Kresse and J. Furthmüller, *Phys. Rev. B* **54**, 11169 (1996).
- ²³T. Takeda and S. Ohara, *J. Phys. Soc. Jpn.* **37**, 275 (1974).
- ²⁴G. Kresse and D. Joubert, *Phys. Rev. B* **59**, 1758 (1999).
- ²⁵J. P. Perdew, K. Burke, and M. Ernzerhof, *Phys. Rev. Lett.* **77**, 3865 (1996).
- ²⁶M. R. Hestenes and E. Stiefel, *J. Res. Natl. Bur. Stand.* **49**, 409 (1952).
- ²⁷J. F. Ding, O. I. Lebedev, S. Turner, Y. F. Tian, W. J. Hu, J. W. Seo, C. Panagopoulos, W. Prellier, G. Van Tendeloo, and T. Wu, *Phys. Rev. B* **87**, 054428 (2013).
- ²⁸M. Vafaei, S. Finizio, H. Deniz, D. Hesse, H. Zabel, G. Jakob, and M. Klaui, *Appl. Phys. Lett.* **108**, 072401 (2016).
- ²⁹J. F. Ding, Y. F. Tian, W. J. Hu, W. N. Lin, and T. Wu, *Appl. Phys. Lett.* **102**, 032401 (2013).
- ³⁰K. Nadeem, W. Zhang, D. Y. Chen, Z. A. Ren, and X. G. Qiu, *Sci. Rep.* **5**, 10700 (2015).
- ³¹A. Bhattacharyya, S. Giri, and S. Majumdar, *Phys. Rev. B* **83**, 134427 (2011).